Hydrogel-derived VPO_4/porous carbon framework for enhanced lithium and sodium storage

Donglei Guo[a], Mengke Yang[a], Yicong Li[a], Yuwen xue[a], Guilong Liu[a], Naiteng Wu[a,c], Jang-Kyo Kim*[b] and Xianming Liu*[a]

[a] Key Laboratory of Function-oriented Porous Materials, College of Chemistry and Chemical Engineering, Luoyang Normal University, Luoyang, 471934, P. R. China.

[b] Department of Mechanical and Aerospace Engineering, Hong Kong University of Science and Technology, Clear Water Bay, Kowloon, Hong Kong, P. R. China.

[c] College of Materials and Chemical Engineering, China Three Gorges University, Yichang, 443002, P. R. China.

*Email: myclxm@163.com (Xianming Liu) & mejkkim@ust.hk (Jang-Kyo Kim)

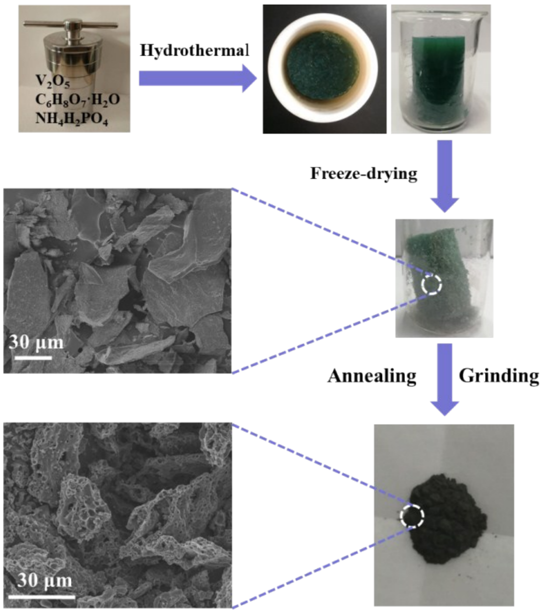

Fig. S1. Digital photographs and FESEM images of precursor sample material after freeze-drying and 3DHP-VPO_4@C.

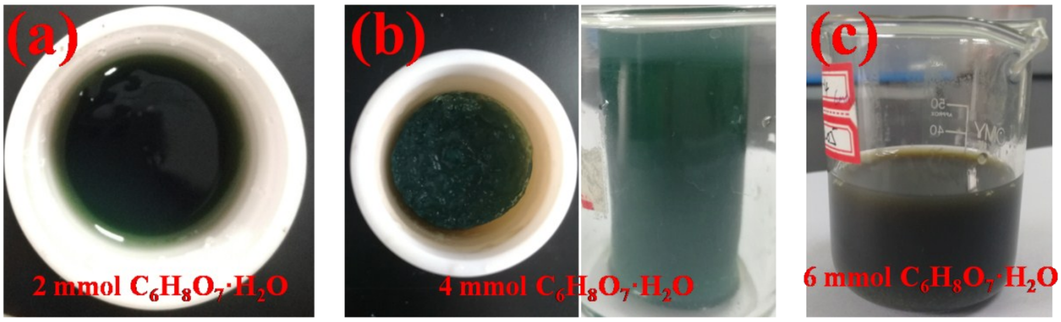

Fig. S2. Digital photographs of hybrid hydrogel obtained after hydrothermal treatment for different $C_6H_8O_7 \cdot H_2O$ contents of (a) 2, (b) 4 and (c) 6 mmol.

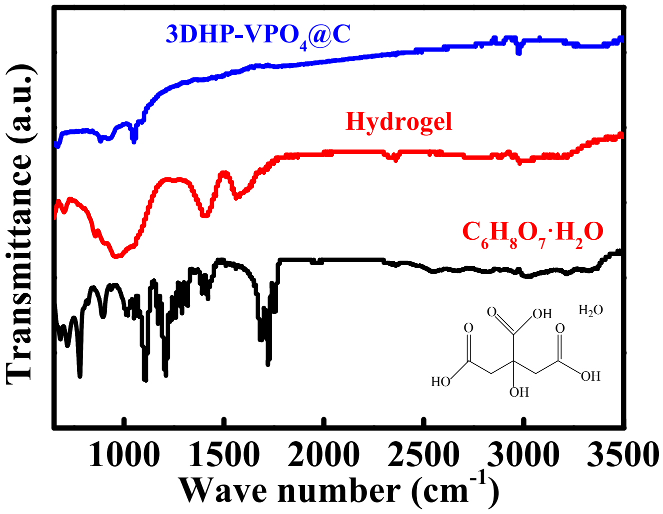

Fig. S3. FT-IR spectras of $C_6H_8O_7{\cdot}H_2O$, hydrogel and 3DHP-VPO_4@C.

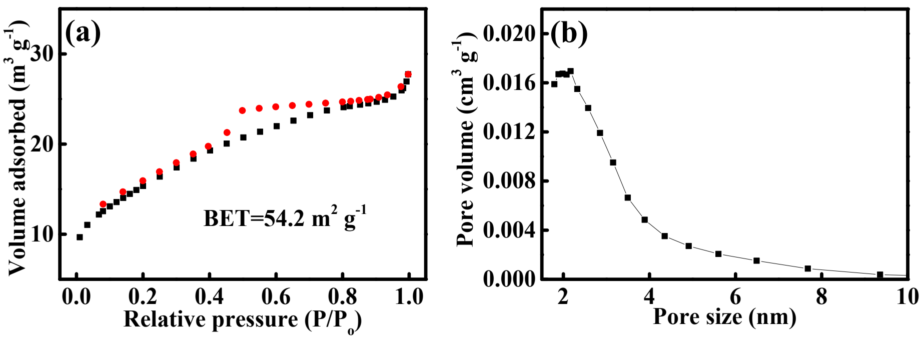

Fig. S4. N_2 adsorption-desorption isotherm (a) and pore size distribution (b) of 3DHP-VPO_4@C according to the NLDFT model.

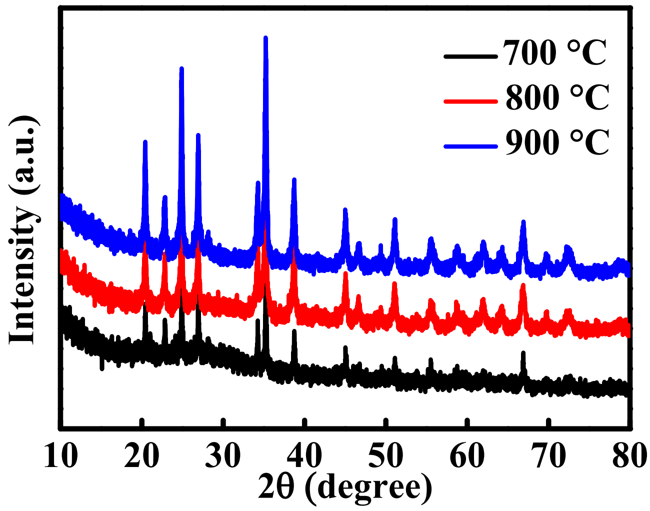

Fig. S5. XRD patterns of VPO_4@C calcined at 700, 800 and 900 ℃.

All XRD peaks of 3DHP-VPO_4@C, VPO_4@C-700 and VPO_4@C-900 can be assigned to the orthorhombic VPO_4 phase (PDF#076-2023).

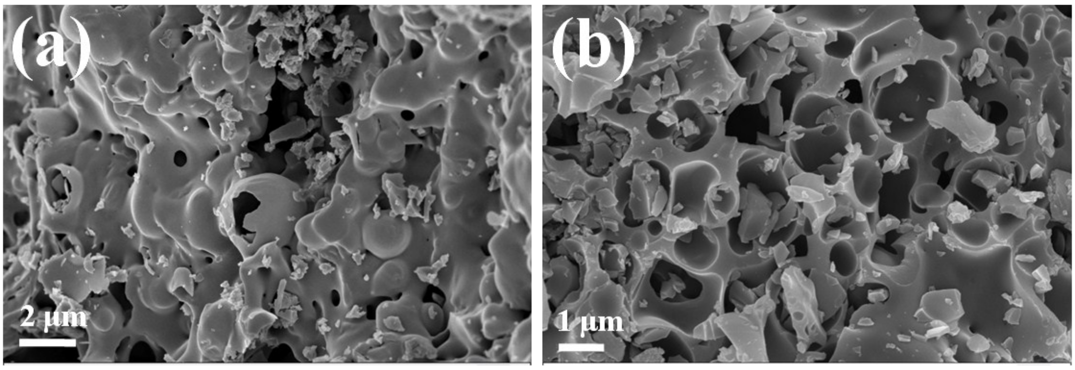

Fig. S6. FESEM images of VPO_4@C calcined at 700 (a) and 900 ℃ (b).

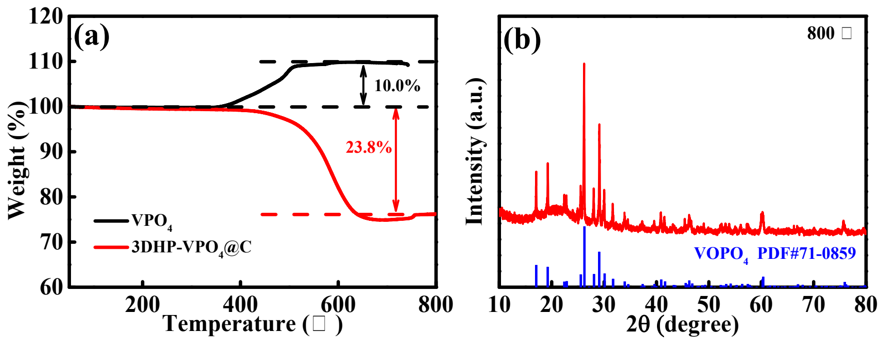

Fig. S7. (a) TGA curves of 3DHP-VPO_4@C and VPO_4 in the temperature range of 30-800 °C in the flowing of air atmosphere; (b) XRD pattern for final product of VPO_4 sintered at 800 °C under air atmosphere.

The TGA test is operated in air flow to calculate the carbon content of 3DHP-VPO_4@C. The apparent increasing mass of VPO_4 is corresponded to the oxidation of VPO_4 to $VOPO_4$ (**Fig. S6b**). In contrast, the rapid mass loss for 3DHP-VPO_4@C is related to the removal of carbonous materials. The carbon content in 3DHP-VPO_4@C is determined to be 33.8 wt%.

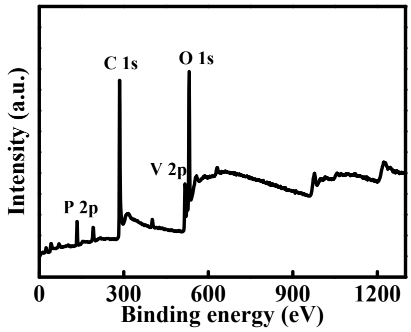

Fig. S8. XPS curves of survey spectrum of 3DHP-VPO_4@C.

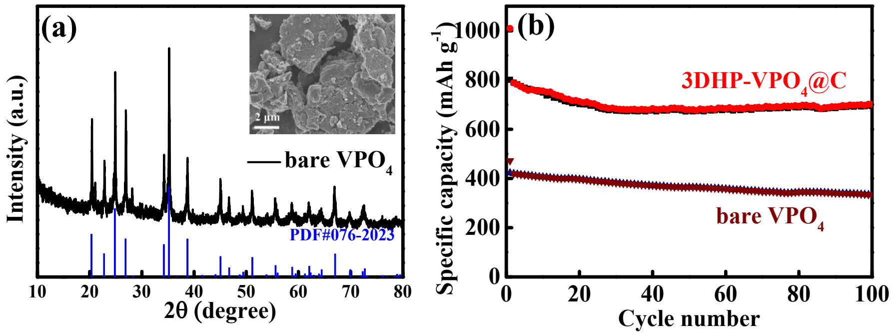

Fig. S9. (a) XRD pattern of bare VPO_4 and the inset is its FESEM image; (b) The cycling performances of 3DHP-VPO_4@C and bare VPO_4 at 100 mA g^{-1}.

Table S1. Comparison of electrochemical performance between the current electrode and state-of-the-art VPO_4-based electrodes.

VPO_4-based electrodes	Current density (mA g^{-1})/Rate	Initial specific capacity (mA h g^{-1})	Cycle number	Specific capacity (mA h g^{-1})	Ref.
VPO_4/C/Ag	0.2 C	857.8	100	324.2	[S1]
VPO_4/C/3DG	0.2 C	976.8	30	632	[S2]
	5 C	369	100	338.8	
a-VPO_4/C	200	1094.6	50	804.5	[S3]
Nano-sheets-VPO_4	0.05 C	788.7			[S4]
Core-shell VPO_4/C	20	887.3	30	343	[S5]
MVHP-VPO_4@C NSs	100	943	100	630	[S6]
VPO_4@C/rGO	100	1074	100	395.3	[S7]
VPO_4/rGO	100	567	100	475	[S8]
Current work (3DHP-VPO_4@C)	100	1009.4	100	700.5	
	2000	542.1	2000	288.5	

Table S2. Impedance parameters of 3DHP-VPO_4@C, VPO_4@C-700 and VPO_4@C-900 electrodes fitted with the circuit model of R(QR)(QR)W.

Electrodes	R_s (Ω)	R_{ct}(Ω)	Z_w (Ω)
3DHP-VPO_4@C	3.5	20.4	1.5
VPO_4@C-700	7.4	46.7	5.4
VPO_4@C-900	5.2	27.6	2.8

[S1] L.Z. Hu, S. Zheng, S.Q. Cheng, Z. Chen, B. Huang, Q.Q. Liu, Q.Q. Chen, Micro/nano-structured Ag coated VPO_4/C as a high-performance anode material for lithium-ion batteries, Mater. Lett. 2019, 246, 40-44.

[S2] L.Z. Hu, S. Zheng, Z. Chen, B. Huang, J.W. Yang, Q.Q. Chen, 3D graphene modified sphere-like VPO_4/C as a high-performance anode material for lithium-ion batteries, Electrochim. Acta 2018, 284, 609-617.

[S3] X.H. Nan, C.F. Liu, K. Wang, W.D. Ma, C.K. Zhang, H.Y. Fu, Z.Y. Li, G.Z. Cao, Amorphous VPO_4/C with the enhanced performances as an anode for lithium ion batteries, J. Materiomics 2016, 2, 350-357.

[S4] J.C. Zheng, Y.D. Han, B. Zhang, C. Shen, L. Ming, X. Ou, J.F. Zhang, Electrochemical Properties of VPO_4/C Nanosheets and Microspheres As Anode Materials for Lithium-Ion Batteries, ACS Appl. Mater. Interfaces 2014, 6, 6223-6226.

[S5] Y. Zhang, X.J. Zhang, Q. Tang, D.H. Wu, Z. Zhou, Core-shell VPO_4/C anode materials for Li ion batteries: Computational investigation and sol-gel synthesis, J. Alloy. Compd. 2012, 522, 167-171.

[S6] D. Zhao, T. Meng, J.W. Qin, W. Wan g, Z.G. Yin, M.H. Cao, Rational Construction of Multivoids-Assembled Hybrid Nanospheres Based on VPO_4 Encapsulated in Porous Carbon with Superior Lithium Storage Performance, ACS Appl. Mater. Interfaces 2017, 9, 1437-1445.

[S7] L.B. Tang, B. Xiao, C.S. An, H. Li, Z.J. He, J.C. Zheng, VPO_4@C/graphene microsphere as a potential anode material for lithiumion batteries, Ceram. Int. 2018, 44, 14432-14438.

[S8] W. Lu, L.N. Cong, Y.L. Liu, J. Liu, A. Mauger, C.M. Julien, L.Q. Sun, H.M. Xie, Pseudocapacitance controlled fast-charging and long-life lithium ion battery achieved via a 3D mutually embedded VPO4/rGO electrode, J. Alloy. Comp. 2020, 812, 152135.